

Quantitative test of the time dependent Ginzburg-Landau equation for sheared granular flow in two dimension

Kuniyasu Saitoh*

Faculty of Engineering Technology, University of Twente, Enschede, the Netherlands

Hisao Hayakawa†

Yukawa Institute for Theoretical Physics, Kyoto University, Sakyo-ku, Kyoto, Japan

(Dated: June 4, 2019)

We examine the validity of the time-dependent Ginzburg-Landau equation of granular fluids for a plane shear flow under the Lees-Edwards boundary condition derived from a weakly nonlinear analysis through the comparison with the result of discrete element method. We verify quantitative agreements in the time evolution of the area fraction and the vertical component to the sheared direction of the velocity field, and also found qualitative agreements in the velocity field in the sheared direction and the granular temperature.

I. INTRODUCTION

Flows of granular particles have been extensively studied due to the importance in powder technology, civil engineering, mechanical engineering, geophysics, astrophysics, and applied mathematics and physics [1–4]. The characteristic properties of the granular flows are mainly caused by the inelastic collisions [5]. In particular, the study of granular gases under a plane shear plays an important role in the application of the kinetic theory [6–15], the shear band in a moderate dense flow [16, 17], the long-time tail and the long-range correlations [18–27], the pattern formation of dense flow [28–33], the determination of the constitutive equation for dense flow [34–36], as well as jamming transition [37–43].

The granular hydrodynamic equations based on the kinetic theory well describe the dynamics of moderate dense granular gases [8–15], even though its applicability is questionable because of the lack of scale separation and the existence of long range correlations, etc. The two-dimensional granular shear flow is an appropriate subject to check the validity of the granular hydrodynamic equations, where two shear bands are formed near the boundary and collide to form a shear band under a physical boundary condition [16, 17]. A similar shear band is also observed under the Lees-Edwards boundary condition. The transient dynamics of the shear band and the hydrodynamic fields can be described by the granular hydrodynamic equations, where reasonable agreements with the discrete element method (DEM) simulation have been verified [17]. It is also known that a homogeneous state of the two-dimensional granular shear flow is intrinsically unstable as predicted by the linear stability analysis [44–50].

To understand the shear band formation after the homogeneous state becomes unstable, we have to develop the weakly nonlinear analysis. Recently, Shukla and Alam carried out a weakly nonlinear analysis of the sheared granular flow in finite size systems, where they derived the Stuart-Landau type equation for the disturbance amplitude of the hydrodynamic fields under a physical boundary condition [51–53]. They found the existence of subcritical bifurcation in both dilute and dense regimes, while a supercritical bifurcation appears in the medium regime and the extremely dilute regime. The Stuart-Landau equation, however, does not include any spatial degrees of freedom and cannot be used to study the slow evolution of the spatial structure of shear band. We also notice that the shear rate is fixed to unity and cannot be used as a control parameter in their analysis.

It is also notable that Khain found the coexistence of the solid and liquid phases in his molecular dynamics simulation of a dense granular shear flow [32, 33]. He demonstrated the existence of a hysteresis loop of the order parameter defined as the difference of the densities between the boundary and the center region. It should be noted, however, that the mechanism of the subcritical bifurcation based on a set of hydrodynamic equations differs from that observed in the jamming transition of frictional particles [43].

In our previous work, we have developed the weakly nonlinear analysis for the two-dimensional granular shear flow and derived the time dependent Ginzburg-Landau (TDGL) equation for the disturbance amplitude. We introduced a hybrid approach to the weakly nonlinear analysis, where the derived TDGL equation is written as a two-dimensional

*k.saitoh@utwente.nl; <http://www2.msm.ctw.utwente.nl/saitohk/>

†hisao@yukawa.kyoto-u.ac.jp

form and has time dependent diffusion coefficients [54]. We have also discussed the bifurcation of the amplitude, however, the studies of the numerical solution of the TDGL equation and comparison with the DEM simulation had been left as an incomplete part of our previous paper [54].

In this paper, we quantitatively examine the validity of the derived TDGL equation for a two dimensional granular shear flow from the comparison with the DEM simulation. In Sec. II, we review the weakly nonlinear analysis and the hybrid approach. In Sec. III, we compare the numerical solutions of the TDGL equation with the results of DEM simulation. In Sec. IV, we discuss and conclude our results.

II. OVERVIEW OF WEAKLY NONLINEAR ANALYSIS

In this section, we review our previous results for the weakly nonlinear analysis, where the time evolution for the disturbance amplitude is described by the TDGL equation [54]. We also apply the hybrid approach to the TDGL equation to describe the structural changes of the shear band [54]. In Sec. IIA, we introduce the basic equations. In Sec. IIB, we review the weakly nonlinear analysis to derive the TDGL equation. In Sec. IIC, we derive a two-dimensional TDGL equation adopting the hybrid approach to the weakly nonlinear analysis.

A. Basic equations

Let us explain our setup and basic equations. To avoid difficulties caused by the physical boundary condition, we adopt the Lees-Edwards boundary condition [55], where the upper and the lower image cells move to the opposite directions with a constant speed $U/2$. Here, the distance between the upper and the lower image cells is given by L . We assume that the granular disks are identical, where the mass, the diameter and the restitution coefficient are respectively given by m , d and e . In the following argument, we scale the mass, the length and the time by m , d and $2d/U$, respectively. Therefore, the shear rate U/L is nondimensionalized as $\epsilon \equiv 2d/L$ which becomes a small parameter in the hydrodynamic limit $L \gg d$.

We employ a set of hydrodynamic equations of granular disks derived by Jenkins and Richman [14]. Although their original equations include the angular momentum and the spin temperature, it is known that the spin effects are localized near the boundary [56] and the effect of rotation can be absorbed in the normal restitution coefficient, if the friction constant is small [17, 57, 58]. Thus, our system is reduced to a system without the spin effects and the dimensionless hydrodynamic equations are given by

$$(\partial_t + \mathbf{v} \cdot \nabla) \nu = -\nu \nabla \cdot \mathbf{v} \quad (1)$$

$$\nu (\partial_t + \mathbf{v} \cdot \nabla) \mathbf{v} = -\nabla \cdot \mathbf{P} \quad (2)$$

$$(\nu/2) (\partial_t + \mathbf{v} \cdot \nabla) \theta = -\mathbf{P} : \nabla \mathbf{v} - \nabla \cdot \mathbf{q} - \chi, \quad (3)$$

where ν , $\mathbf{v} = (u, w)$, θ , t and $\nabla = (\partial/\partial_x, \partial/\partial_y)$ are the area fraction, the dimensionless velocity fields, the dimensionless granular temperature, the dimensionless time and the dimensionless gradient, respectively. The pressure tensor $\mathbf{P} = (P_{ij})$, the heat flux \mathbf{q} and the energy dissipation rate χ are given in the dimensionless forms as

$$P_{ij} = \left[p(\nu)\theta - \xi(\nu)\theta^{1/2} (\nabla \cdot \mathbf{v}) \right] \delta_{ij} - \eta(\nu)\theta^{1/2} e_{ij}, \quad (4)$$

$$\mathbf{q} = -\kappa(\nu)\theta^{1/2} \nabla \theta - \lambda(\nu)\theta^{3/2} \nabla \nu, \quad (5)$$

$$\chi = \frac{1-e^2}{4\sqrt{2\pi}} \nu^2 g(\nu) \theta^{1/2} \left[4\theta - 3\sqrt{\frac{\pi}{2}} \theta^{1/2} (\nabla \cdot \mathbf{v}) \right], \quad (6)$$

respectively, where $p(\nu)\theta$, $\xi(\nu)\theta^{1/2}$, $\eta(\nu)\theta^{1/2}$, $\kappa(\nu)\theta^{1/2}$ and $\lambda(\nu)\theta^{3/2}$ are the dimensionless forms of the static pressure, the bulk viscosity, the shear viscosity, the heat conductivity and the coefficient associated with the gradient of density, respectively, and $e_{ij} \equiv (\nabla_j v_i + \nabla_i v_j - \delta_{ij} \nabla \cdot \mathbf{v})/2$ ($i, j = x, y$) is the deviatoric part of the strain rate tensor. The explicit forms of them are listed in Table I, where we adopt the radial distribution function at contact

$$g(\nu) = \frac{1 - 7\nu/16}{(1 - \nu)^2}, \quad (7)$$

which is only valid for $\nu < 0.7$ [59–62].

$$\begin{aligned}
p(\nu) &= \frac{1}{2}\nu [1 + (1+e)\nu g(\nu)] \\
\xi(\nu) &= \frac{1}{\sqrt{2\pi}}(1+e)\nu^2 g(\nu) \\
\eta(\nu) &= \sqrt{\frac{\pi}{2}} \left[\frac{g(\nu)^{-1}}{7-3e} + \frac{(1+e)(3e+1)}{4(7-3e)}\nu + \left(\frac{(1+e)(3e-1)}{8(7-3e)} + \frac{1}{\pi} \right) (1+e)\nu^2 g(\nu) \right] \\
\kappa(\nu) &= \sqrt{2\pi} \left[\frac{g(\nu)^{-1}}{(1+e)(19-15e)} + \frac{3(2e^2+e+1)}{8(19-15e)}\nu + \left(\frac{9(1+e)(2e-1)}{32(19-15e)} + \frac{1}{4\pi} \right) (1+e)\nu^2 g(\nu) \right] \\
\lambda(\nu) &= -\sqrt{\frac{\pi}{2}} \frac{3e(1-e)}{16(19-15e)} [4(\nu g(\nu))^{-1} + 3(1+e)] \frac{d(\nu^2 g(\nu))}{d\nu}
\end{aligned}$$

TABLE I: The functions in Eqs.(4)-(6).

B. Weakly nonlinear analysis

To study the slow dynamics of shear band, we need to develop a weakly nonlinear analysis. For this purpose, we introduce a long time scale $\tau \equiv \epsilon^2 t$ and long length scales $(\xi, \zeta) \equiv \epsilon(x, y)$. We also introduce the neutral solution around the most unstable mode $\mathbf{q}_c = (0, q_c)$ as

$$\hat{\phi}_n = A^L(\zeta, \tau) \phi_{q_c}^L e^{iq_c \zeta} + \text{c.c.}, \quad (8)$$

where c.c. represents the complex conjugate and $\phi_{q_c}^L$ is the Fourier coefficient at \mathbf{q}_c . We notice that the amplitude of the layering mode $A^L(\zeta, \tau)$ depends only on ζ but is independent on ξ , because any non-layering modes $q_x \neq 0$ are linearly stable. Then, we expand $A^L(\zeta, \tau)$ into the series of ϵ as

$$A^L(\zeta, \tau) = \epsilon A_1^L + \epsilon^2 A_2^L + \epsilon^3 A_3^L + \dots \quad (9)$$

Substituting Eqs. (8) and (9) into the hydrodynamic equations (1)-(3) and collecting terms in each order of ϵ we obtain an amplitude equation.

The first non-trivial equation at $O(\epsilon^3)$ is the TDGL equation

$$\partial_\tau A_1^L = \sigma_c A_1^L + D \partial_\zeta^2 A_1^L + \beta A_1^L |A_1^L|^2, \quad (10)$$

where D and β are listed in Table 2 of Ref. [54]. Here, σ_c is the maximum growth rate at \mathbf{q}_c scaled by ϵ^2 . Because of the scaling relations $D = \bar{D}$ and $\beta = \epsilon \bar{\beta}$, we can rewrite the TDGL equation as the equation for the scaled amplitude $\bar{A}_1^L \equiv \epsilon^{1/2} A_1^L$ as

$$\partial_\tau \bar{A}_1^L = \sigma_c \bar{A}_1^L + \bar{D} \partial_\zeta^2 \bar{A}_1^L + \bar{\beta} \bar{A}_1^L |\bar{A}_1^L|^2. \quad (11)$$

It should be noted that the TDGL equation (10) or (11) can be only used for $\beta, \bar{\beta} < 0$, i.e., the case of a supercritical bifurcation.

Developing a similar procedure till $O(\epsilon^5)$, we also obtain the amplitude equation

$$\partial_\tau \check{A}^L = \sigma_c \check{A}^L + \bar{D} \partial_\zeta^2 \check{A}^L + \bar{\beta} \check{A}^L |\check{A}^L|^2 + \epsilon \bar{\gamma} \check{A}^L |\check{A}^L|^4 + O(\epsilon^3), \quad (12)$$

where we have introduced $\check{A}^L(\zeta, \tau) = \epsilon^{1/2} [A_1^L(\zeta, \tau) + \epsilon A_2^L(\zeta, \tau) + \epsilon^2 A_3^L(\zeta, \tau)]$ and $\bar{\gamma}$ is also listed in Table 2 of Ref. [54]. Equation (12) can be used for $\bar{\beta} > 0$ and $\bar{\gamma} < 0$, i.e., the case of a subcritical bifurcation.

C. Hybrid approach to the weakly nonlinear analysis

Although we derived the TDGL equations (11) and (12), these equations do not include ξ and they are still not appropriate to study the two-dimensional structure of shear band. Therefore, we need a new approach, where the non-layering mode is coupled with the layering mode. For this purpose, we add a small deviation to the most unstable mode as $\mathbf{q}(\tau) = \mathbf{q}_c + \delta \mathbf{q}(\tau)$ and assume $\hat{\phi}_n$ does not change if the deviation $\delta \mathbf{q}(\tau)$ is small. Then, Eq. (8) can be rewritten as

$$\hat{\phi}_n \simeq A^L(\xi, \zeta, \tau) \phi_{q_c}^L e^{i\mathbf{q}(\tau) \cdot \mathbf{z}} + \text{c.c.}, \quad (13)$$

where we have introduced $\mathbf{z} \equiv (\xi, \zeta)$ and a ξ -dependent amplitude $A^L(\xi, \zeta, \tau)$. If we also take into account the contribution from the non-layering mode, a hybrid solution may be given by

$$\begin{aligned}
\hat{\phi}_h &= \left\{ A^L(\xi, \zeta, \tau) \phi_{q_c}^L + A^{\text{NL}}(\xi, \zeta, \tau) \phi_{\mathbf{q}(\tau)}^{\text{NL}} \right\} e^{i\mathbf{q}(\tau) \cdot \mathbf{z}} + \text{c.c.} \\
&\simeq A(\xi, \zeta, \tau) \left\{ \phi_{q_c}^L + \phi_{\mathbf{q}(\tau)}^{\text{NL}} \right\} e^{i\mathbf{q}(\tau) \cdot \mathbf{z}} + \text{c.c.}, \quad (14)
\end{aligned}$$

where $A^{\text{NL}}(\xi, \zeta, \tau)$ and $\phi_{\mathbf{q}(\tau)}^{\text{NL}}$ are the amplitude and the Fourier coefficient of the non-layering mode, respectively. Here, we have used a strong assumption that $A^{\text{L}}(\xi, \zeta, \tau)$ and $A^{\text{NL}}(\xi, \zeta, \tau)$ are scaled by a common amplitude $A(\xi, \zeta, \tau)$ in the second line of Eq. (14). Expanding $A(\xi, \zeta, \tau)$ as

$$A(\xi, \zeta, \tau) = \epsilon A_1(\xi, \zeta, \tau) + \epsilon^2 A_2(\xi, \zeta, \tau) + \epsilon^3 A_3(\xi, \zeta, \tau) + \dots, \quad (15)$$

and carrying out the weakly nonlinear analysis for the hybrid solution $\hat{\phi}_h$, we found the rescaled amplitude $\bar{A}_1(\xi, \zeta, \tau) \equiv \epsilon^{1/2} A_1(\xi, \zeta, \tau)$ for the supercritical bifurcation satisfies

$$\partial_\tau \bar{A}_1 = \sigma_c \bar{A}_1 + \bar{D}_1(\tau) \partial_\xi^2 \bar{A}_1 + \bar{D}_2(\tau) \partial_\xi \partial_\zeta \bar{A}_1 + \bar{D} \partial_\zeta^2 \bar{A}_1 + \bar{\beta} \bar{A}_1 |\bar{A}_1|^2 \quad (16)$$

at $O(\epsilon^3)$, where $\bar{D}_1(\tau)$ and $\bar{D}_2(\tau)$ are the time dependent diffusion coefficients. Similarly, we found the higher order equation of $\check{A}(\xi, \zeta, \tau) \equiv \epsilon^{1/2} \{A_1(\xi, \zeta, \tau) + \epsilon A_2(\xi, \zeta, \tau) + \epsilon^2 A_3(\xi, \zeta, \tau)\}$ as

$$\partial_\tau \check{A} = \sigma_c \check{A} + \bar{D}_1(\tau) \partial_\xi^2 \check{A} + \bar{D}_2(\tau) \partial_\xi \partial_\zeta \check{A} + \bar{D} \partial_\zeta^2 \check{A} + \bar{\beta} \check{A} |\check{A}|^2 + \epsilon \bar{\gamma} \check{A} |\check{A}|^4 + O(\epsilon^3) \quad (17)$$

for the subcritical bifurcation. The time dependent diffusion coefficients $\bar{D}_1(\tau)$ and $\bar{D}_2(\tau)$ whose explicit forms are given by Eqs. (64) and (65) in Ref. [54] decay to zero as time goes on. Therefore, Eqs. (16) and (17) are respectively reduced to Eqs. (11) and (12) in the long time limit.

III. DISCRETE ELEMENT METHOD (DEM) SIMULATION

In this section, we perform the discrete element method (DEM) simulation for a two-dimensional granular shear flow to compare the results with the weakly nonlinear analysis. In Sec. III A, we introduce our setup and in Sec. III B, we show the time evolution of the density field obtained from the DEM simulation, where the typical transient dynamics can be reproduced. In Sec. III C, we exhibit the time evolution of the velocity fields and the granular temperature, and in Sec. III D, we compare the results of the DEM simulation with the numerical solution of the TDGL equation. In the following, we use the same units of mass, length and time as those in the weakly nonlinear analysis.

In Eq. (16), $\bar{\beta} < 0$ for $\nu_0 < 0.245$ where the supercritical bifurcation is expected [54]. If $0.245 < \nu_0 < 0.275$, $\bar{\beta} > 0$ and $\bar{\gamma} < 0$, thus Eq. (17) should be used and the subcritical bifurcation is expected. Unfortunately, $\bar{\beta} > 0$ and $\bar{\gamma} > 0$ for $\nu_0 > 0.275$ and neither Eqs. (16) nor (17) can be used. Therefore, we exhibit our results with $\nu_0 = 0.18$ for the supercritical case, and with $\nu_0 = 0.26$ for the subcritical case, respectively.

A. Setup

We adopt the linear spring-dashpot model, where the normal force between the colliding two particles is $f_n = k_n \delta - \eta_n \dot{\delta}$ with the overlap δ and the relative speed $\dot{\delta}$. For simplicity, we ignore the tangential contact force, because we have already verified the results are unchanged for the realistic value of the friction coefficient by introducing the effective restitution coefficient. In our units, the spring and viscosity constants are respectively $k_n = 500mU^2/d^2$ and $\eta_n = 1.0mU/d$, and the normal restitution coefficient is $e = 0.9$. The periodic boundary condition and the Lees-Edwards boundary condition with the relative speed U are adopted for the boundaries of the ξ - and ζ -axes, respectively. Then, we randomly distribute $N = 8192$ particles in a $L^* \times L^*$ square box with the dimensionless system size $L^* \equiv L/d = 189$ ($\nu_0 = 0.18$) and 155 ($\nu_0 = 0.26$), respectively, and randomly distribute the initial velocities around the linear velocity profile with the dimensionless shear rate $\epsilon \simeq 10^{-2}$.

B. Shear band formation

Figure 1 (*upper panel*) displays the time evolution of particles in the DEM simulation for $\nu_0 = 0.18$. The hydrodynamic fields can be obtained by the coarse graining (CG) procedure developed by Goldhirsch et. al. [63–72], where the CG function is defined as $\psi(\mathbf{z}) = e^{-\mathbf{z}^2}/\pi$ at $\mathbf{z} = (\xi, \zeta)$. Figure 1 (*middle panel*) shows the time evolution of the area fraction defined as

$$\nu_{\text{DEM}}(\mathbf{z}, \tau) = \sum_{i=1}^N s \psi(\mathbf{z} - \mathbf{z}_i), \quad (18)$$

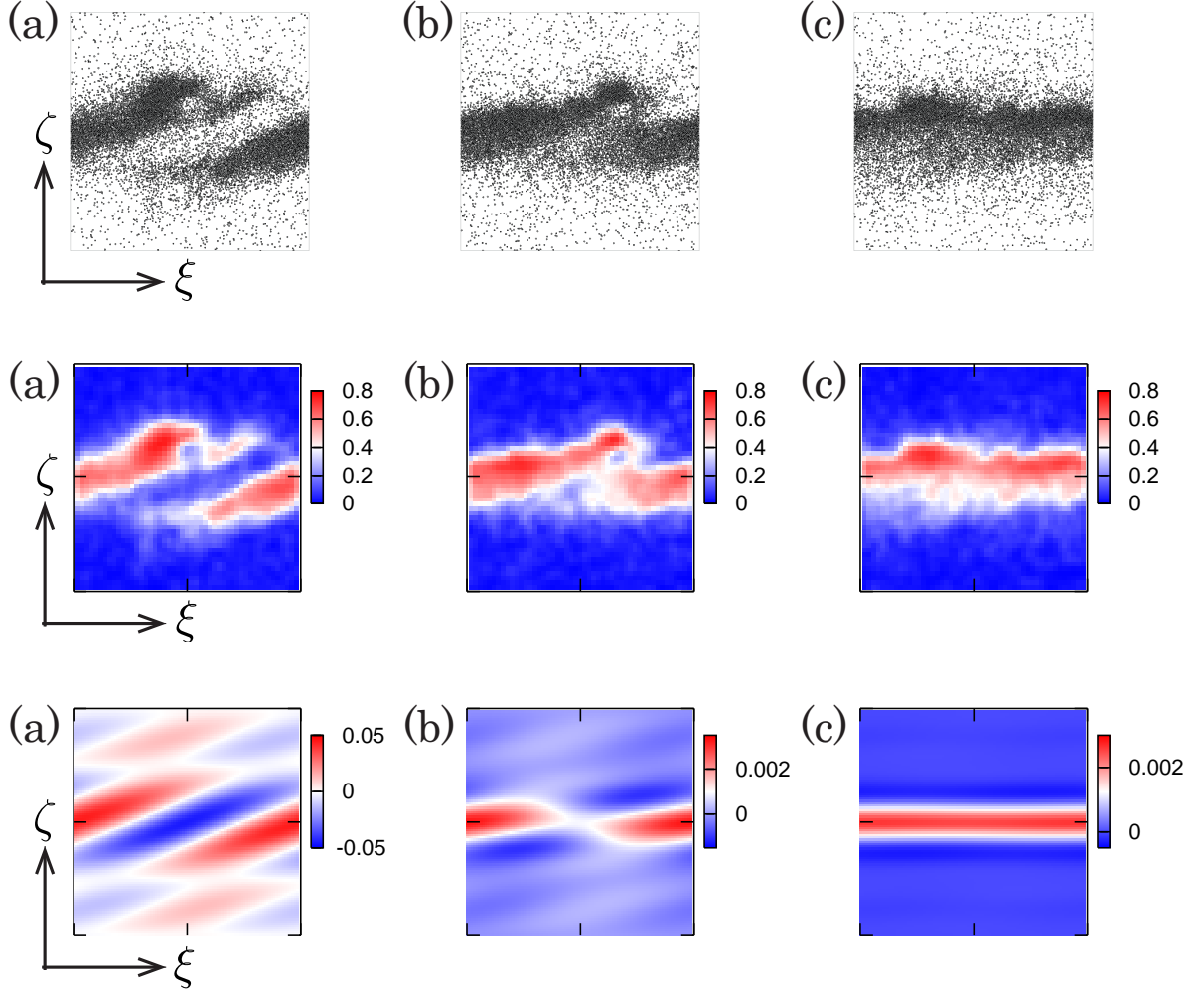


FIG. 1: (Color online) *Upper panel*: Time evolution of particles in the DEM simulation, where $\nu_0 = 0.18$. *Middle panel*: Time evolution of $\nu_{\text{DEM}}(\mathbf{z}, \tau)$. *Lower panel*: Numerical solution of Eq. (16). Here, the dimensionless time corresponds to (a) 4.8, (b) 11.2 and (c) 20.0, respectively.

where $\mathbf{z}_i = (\xi_i, \zeta_i)$ and $s = \pi/4$ are the dimensionless position of the i -th particle and the dimensionless area of a particle, respectively. Figure 1 (*lower panel*) shows the numerical solution of Eq. (16).

In Fig. 1, a typical transient dynamics exhibits that (a) the fluctuation with the short wave length is suppressed, (b) clusters are generated and merged, and (c) the shear band is generated and the system reaches a steady state. Such transient dynamics of shear band is qualitatively similar to the numerical solution of Eq. (16). We should stress that these results cannot be explained by neither the one-dimensional TDGL equation nor zero-dimensional Stuart-Landau equation obtained by the ordinary weakly nonlinear analysis [51–53].

C. Velocity fields and granular temperature

The velocity fields and the granular temperature are defined as

$$\mathbf{u}_{\text{DEM}}(\mathbf{z}, \tau) = \frac{\sum_i \mathbf{v}_i \psi(\mathbf{z} - \mathbf{z}_i)}{\sum_i \psi(\mathbf{z} - \mathbf{z}_i)}, \quad (19)$$

$$\theta_{\text{DEM}}(\mathbf{z}, \tau) = \frac{\sum_i \mathbf{V}_i^2 \psi(\mathbf{z} - \mathbf{z}_i)}{2 \sum_i \psi(\mathbf{z} - \mathbf{z}_i)}, \quad (20)$$

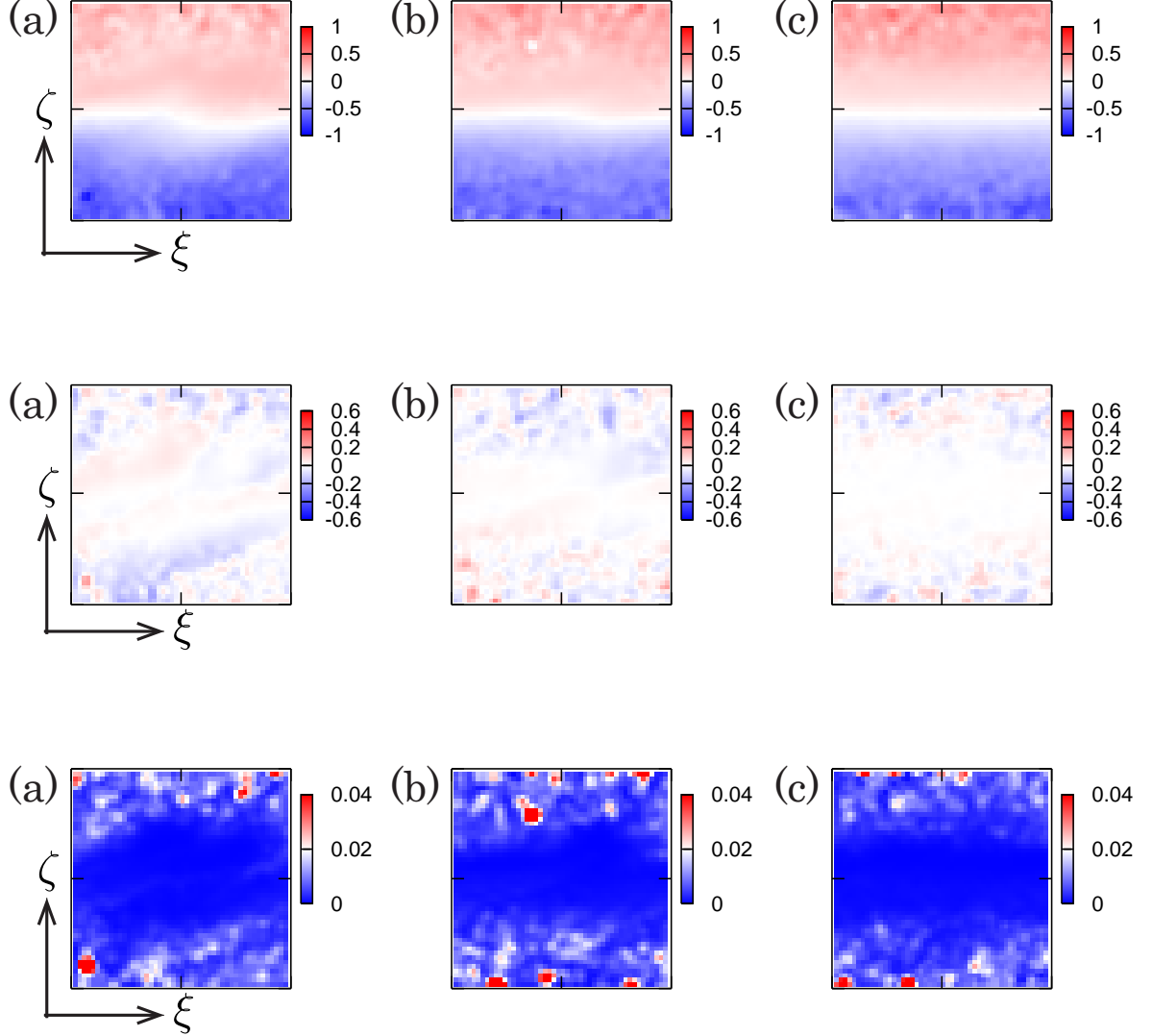


FIG. 2: (Color online) *Upper panel*: Time evolution of $u_{\text{DEM}}(\mathbf{z}, \tau)$. *Middle panel*: Time evolution of $w_{\text{DEM}}(\mathbf{z}, \tau)$. *Lower panel*: Time evolution of $\theta_{\text{DEM}}(\mathbf{z}, \tau)$. Here, the dimensionless time corresponds to (a) 4.8, (b) 11.2 and (c) 20.0, respectively.

respectively, where \mathbf{v}_i and $\mathbf{V}_i = \mathbf{v}_i - \mathbf{u}_{\text{DEM}}(\mathbf{z}_i, \tau)$ are the dimensionless velocity of the i -th particle and the dimensionless local velocity, respectively. Figures 2 (*upper panel*), (*middle panel*) and (*lower panel*) display the time evolution of $u_{\text{DEM}}(\mathbf{z}, \tau)$, $w_{\text{DEM}}(\mathbf{z}, \tau)$ and $\theta_{\text{DEM}}(\mathbf{z}, \tau)$, respectively, where $u_{\text{DEM}}(\mathbf{z}, \tau)$ and $w_{\text{DEM}}(\mathbf{z}, \tau)$ are respectively the ξ and ζ components of $\mathbf{u}_{\text{DEM}}(\mathbf{z}, \tau)$. As time goes on, $u_{\text{DEM}}(\mathbf{z}, \tau)$ in the ζ direction deviates from the linear profile and $w_{\text{DEM}}(\mathbf{z}, \tau)$ is almost homogeneous. The time evolution of $\theta_{\text{DEM}}(\mathbf{z}, \tau)$ is accompanied with $\nu_{\text{DEM}}(\mathbf{z}, \tau)$, where $\theta_{\text{DEM}}(\mathbf{z}, \tau)$ is lower in the dense region and higher in the dilute region.

D. Comparison of the TDGL equation with the DEM simulation

To test the quantitative validity of the TDGL equation, we compare the numerical solution with the results of DEM simulation. At first, we average out $\nu_{\text{DEM}}(\mathbf{z}, \tau)$, $u_{\text{DEM}}(\mathbf{z}, \tau)$, $w_{\text{DEM}}(\mathbf{z}, \tau)$ and $\theta_{\text{DEM}}(\mathbf{z}, \tau)$ over the ξ direction and take sample averages from the different 100 time steps. Then, the hydrodynamic fields are written as one-dimensional forms $\nu_{\text{DEM}}(\zeta, \tau)$, $u_{\text{DEM}}(\zeta, \tau)$, $w_{\text{DEM}}(\zeta, \tau)$ and $\theta_{\text{DEM}}(\zeta, \tau)$, respectively. Because $\nu_{\text{DEM}}(\zeta, \tau)$ and $\theta_{\text{DEM}}(\zeta, \tau)$ are

approximately symmetric at $\zeta = 0$, we introduce

$$\bar{\nu}_{\text{DEM}}(\zeta, \tau) \equiv \frac{1}{2} \{ \nu_{\text{DEM}}(\zeta, \tau) + \nu_{\text{DEM}}(-\zeta, \tau) \} \quad (0 < \zeta < L^*/2), \quad (21)$$

$$\bar{\theta}_{\text{DEM}}(\zeta, \tau) \equiv \frac{1}{2} \{ \theta_{\text{DEM}}(\zeta, \tau) + \theta_{\text{DEM}}(-\zeta, \tau) \} \quad (0 < \zeta < L^*/2), \quad (22)$$

respectively. On the other hand, the velocity fields are approximately antisymmetric at $\zeta = 0$ and we also introduce

$$\bar{u}_{\text{DEM}}(\zeta, \tau) \equiv \frac{1}{2} \{ u_{\text{DEM}}(\zeta, \tau) - u_{\text{DEM}}(-\zeta, \tau) \} \quad (0 < \zeta < L^*/2), \quad (23)$$

$$\bar{w}_{\text{DEM}}(\zeta, \tau) \equiv \frac{1}{2} \{ w_{\text{DEM}}(\zeta, \tau) - w_{\text{DEM}}(-\zeta, \tau) \} \quad (0 < \zeta < L^*/2), \quad (24)$$

respectively.

In the weakly nonlinear analysis, the hydrodynamic fields are given by the summation of the base state $\phi_0 = (\nu_0, \zeta, 0, \theta_0)$ and the hybrid solution $\hat{\phi}_h$. At first, we project $\hat{\phi}_h$ on the ζ -axis as

$$\hat{\phi}_h(\zeta, \tau) \simeq \bar{A}(\zeta, \tau) \phi_{q_c}^L e^{iq_c(\tau)\zeta} + \text{c.c.}, \quad (25)$$

where $q_c(\tau) \equiv q_c - \tau$ is the ζ component of $\mathbf{q}(\tau)$ [73] and we ignore $\phi_{\mathbf{q}(\tau)}^{\text{NL}}$, because $\phi_{\mathbf{q}(\tau)}^{\text{NL}}$ exponentially decays to zero and the following results are unchanged even if we take into account $\phi_{\mathbf{q}(\tau)}^{\text{NL}}$. We note that $\phi_{q_c}^L$ is defined as $\phi_{q_c}^L = (\nu_{q_c}, iu_{q_c}, iw_{q_c}, \theta_{q_c})^T$ with the imaginary unit i , where ν_{q_c} , u_{q_c} , w_{q_c} and θ_{q_c} have been given in our previous study [54]. If we ignore the higher order terms in Eq. (15), $\bar{A}(\zeta, \tau)$ may be given by the numerical solution of Eq. (16) projected on the ζ -axis. Then, the hydrodynamic fields are given by $\phi_{\text{TDGL}}(\zeta, \tau) = \phi_0 + \hat{\phi}_h(\zeta, \tau)$, where each component of $\phi_{\text{TDGL}}(\zeta, \tau)$ is written as

$$\nu_{\text{TDGL}}(\zeta, \tau) = \nu_0 + 2\nu_{q_c} \bar{A}(\zeta, \tau) \cos(q_c(\tau)\zeta), \quad (26)$$

$$u_{\text{TDGL}}(\zeta, \tau) = \zeta - 2u_{q_c} \bar{A}(\zeta, \tau) \sin(q_c(\tau)\zeta), \quad (27)$$

$$w_{\text{TDGL}}(\zeta, \tau) = -2w_{q_c} \bar{A}(\zeta, \tau) \sin(q_c(\tau)\zeta), \quad (28)$$

$$\theta_{\text{TDGL}}(\zeta, \tau) = \theta_0 + 2\theta_{q_c} \bar{A}(\zeta, \tau) \cos(q_c(\tau)\zeta), \quad (29)$$

respectively, where the factor 2 comes from the complex conjugate.

Figures 3 and 4 display the time evolution of the hydrodynamic fields for the supercritical case ($\nu_0 = 0.18$) and the subcritical case ($\nu_0 = 0.26$), respectively, where the symbols represent Eqs. (21)-(24) obtained by the DEM simulation and the lines represent the scaling functions

$$\bar{X}_{\text{TDGL}}(\zeta, \tau) \equiv a_X^* X_{\text{TDGL}}(\zeta/\zeta_X^*(\tau), \tau/\tau^*) \quad (X = \nu, u, w, \theta) \quad (30)$$

with the scaling factors a_X^* , $\zeta_X^*(\tau)$ and τ^* , respectively. In these figures, $\bar{\nu}_{\text{TDGL}}(\zeta, \tau)$ and $\bar{w}_{\text{TDGL}}(\zeta, \tau)$ are quantitatively agreed with $\bar{\nu}_{\text{DEM}}(\zeta, \tau)$ and $\bar{w}_{\text{DEM}}(\zeta, \tau)$, respectively. We should note that we could not get any reasonable agreement between the ζ component of the velocity field in a numerical solution of *full* set of the granular hydrodynamic equations and the result of DEM simulation in our previous work [17]. We can also see the qualitative agreements in the ξ component of the velocity field in the the granular temperature.

IV. DISCUSSION AND CONCLUSION

In this paper, we examine the validity of the TDGL equation for a two-dimensional sheared granular flow from the comparison with the results of the DEM simulation with the aid of the CG method. The results of the TDGL equation, at least, qualitatively agree with the results of the DEM simulation. Such transient dynamics cannot be reproduced by neither the one dimensional TDGL equation nor the zero dimensional Stuart-Landau equation derived by the ordinary weakly nonlinear analysis. We also obtain that the velocity fields and the granular temperature qualitatively agree with the solution of the TDGL equation.

We compare the one dimensional hydrodynamic fields obtained by averaging the results of the DEM simulation with the scaled forms of the numerical solution of the TDGL equation, where we find the qualitative agreements in the area fraction and the velocity field in the ζ direction, while there are still deviations in the velocity field in the ξ direction and the granular temperature. In our previous work, we demonstrated that the hydrodynamic fields

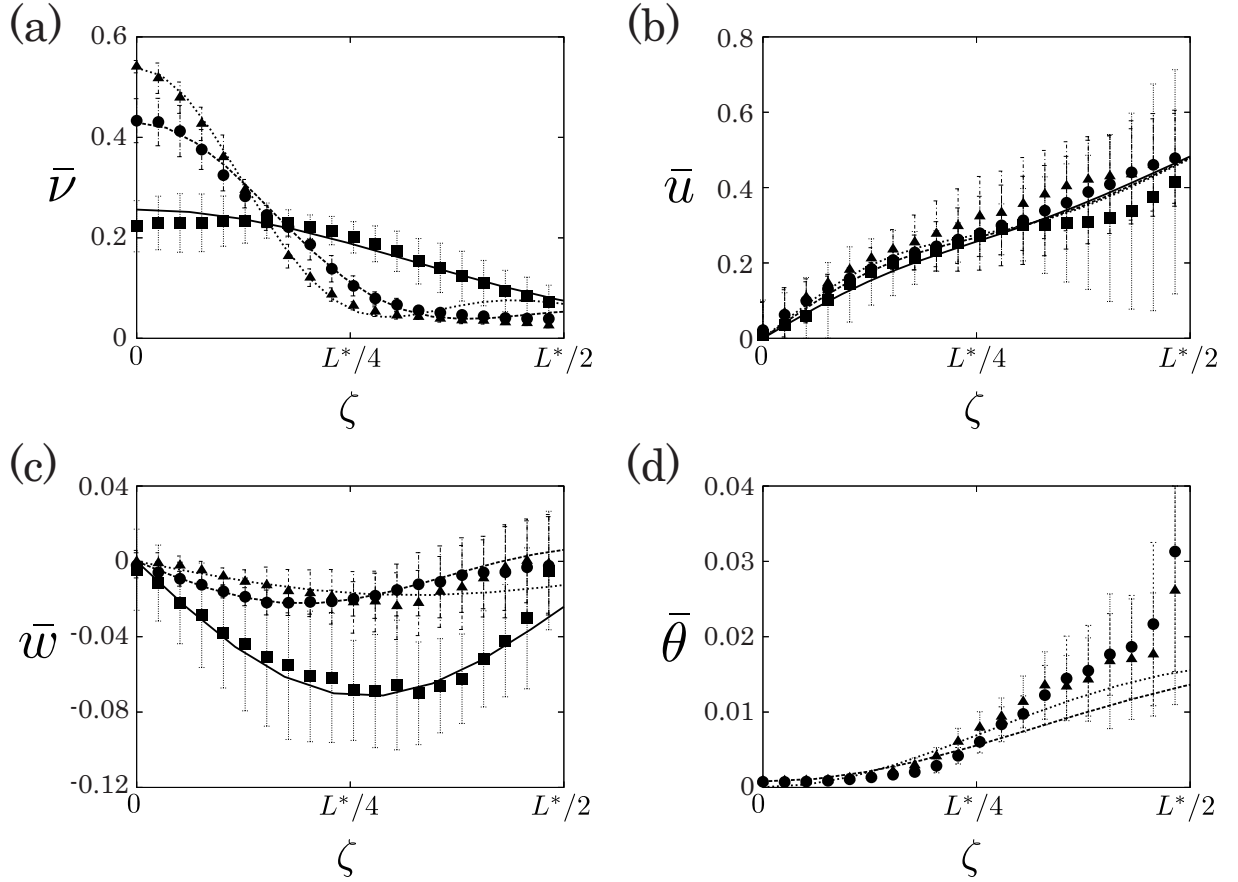


FIG. 3: Time evolution of (a) $\bar{\nu}_{\text{DEM}}(\zeta, \tau)$ and $\bar{\nu}_{\text{TDGL}}(\zeta, \tau)$, (b) $\bar{u}_{\text{DEM}}(\zeta, \tau)$ and $\bar{u}_{\text{TDGL}}(\zeta, \tau)$, (c) $\bar{w}_{\text{DEM}}(\zeta, \tau)$ and $\bar{w}_{\text{TDGL}}(\zeta, \tau)$, (d) $\bar{\theta}_{\text{DEM}}(\zeta, \tau)$ and $\bar{\theta}_{\text{TDGL}}(\zeta, \tau)$, respectively, for the supercritical case ($\nu_0 = 0.18$), where the solid squares and the solid lines correspond to the dimensionless time 4.8, the solid circles and the hashed lines correspond to the dimensionless time 11.2, and the solid triangles and the dotted lines correspond to the dimensionless time 20.0, respectively. Here, we have introduced the scaling factors $\tau^* \simeq 0.14$, $a_\nu^* \simeq 0.24$, $a_u^* \simeq 0.02$, $a_w^* \simeq 1.96$ and $a_\theta^* \simeq 0.02$, respectively, and we also use $\zeta_\nu^*(\tau) \simeq 1.6, 0.9, 0.75$, $\zeta_u^*(\tau) \simeq 0.8, 0.8, 0.8$, $\zeta_w^*(\tau) \simeq 1.5, 1.1, 1.8$ at the dimensionless time 4.8, 11.2 and 20.0, respectively, and $\zeta_\theta^*(\tau) \simeq 1.6, 1.35$ at the dimensionless time 11.2 and 20.0, respectively. It should be noted that we do not show the result of the granular temperature at the dimensionless time 4.8, because it homogeneously distributed around θ_0 and the fluctuation is too large to plot in the same figure.

obtained by the DEM simulation can be reasonably explained by the numerical solution of the *full* hydrodynamic equations by Jenkins and Richmann except for $w(\mathbf{z}, \tau)$ [14, 15, 17]. In the present work, even though we need to introduce the scaling factors, the results of the DEM simulation is qualitatively reproduced by the numerical solution of the TDGL equation. It is needless to say that more precise analyses to remove the scaling factors will be important and is left to our future works.

In conclusion, the numerical solution of the TDGL equation can qualitatively explain the time evolution of the hydrodynamic fields obtained by the DEM simulation.

Acknowledgments

This work was financially supported by an NWO-STW VICI grant. Numerical computation in this work was carried out at the Yukawa Institute Computer Facility.

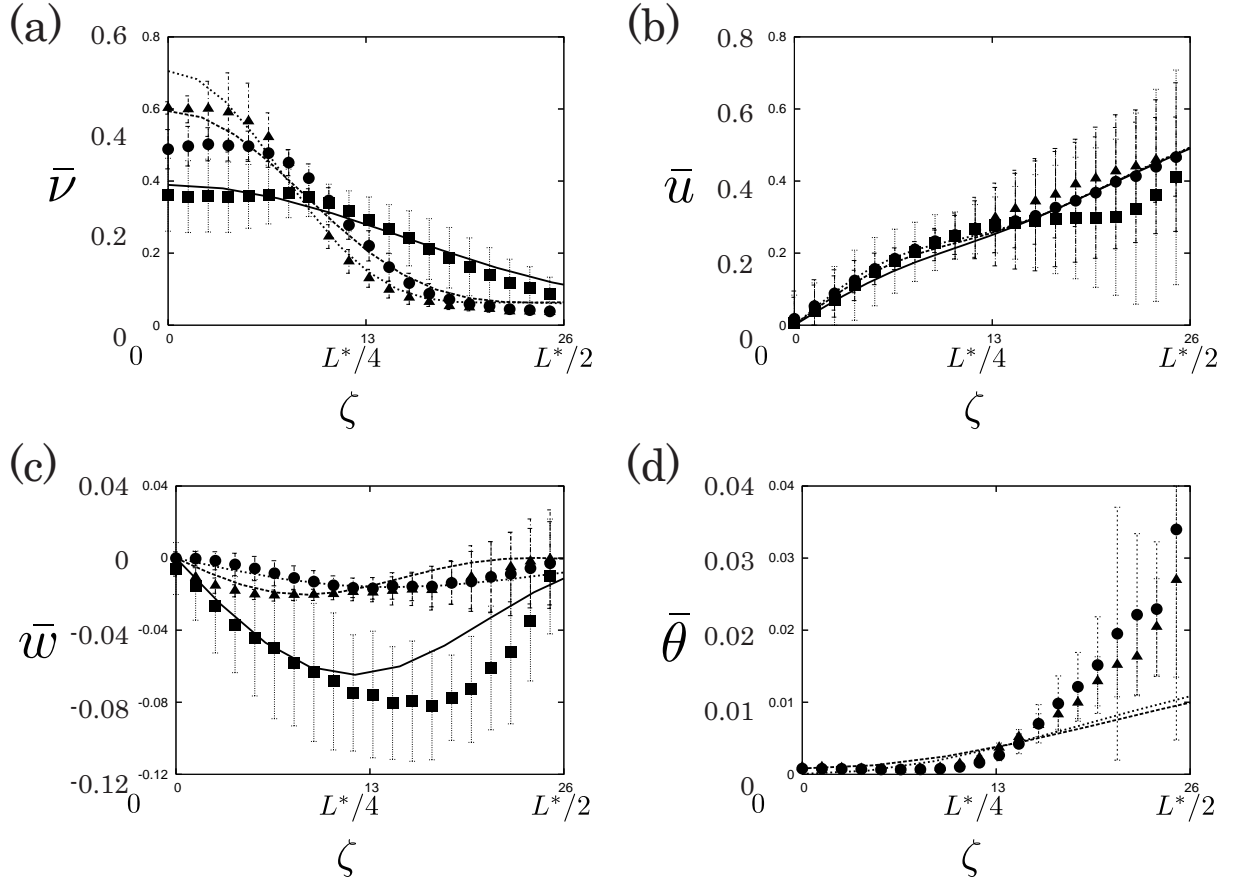


FIG. 4: Time evolution of (a) $\bar{\nu}_{\text{DEM}}(\zeta, \tau)$ and $\bar{\nu}_{\text{TDGL}}(\zeta, \tau)$, (b) $\bar{u}_{\text{DEM}}(\zeta, \tau)$ and $\bar{u}_{\text{TDGL}}(\zeta, \tau)$, (c) $\bar{w}_{\text{DEM}}(\zeta, \tau)$ and $\bar{w}_{\text{TDGL}}(\zeta, \tau)$, (d) $\bar{\theta}_{\text{DEM}}(\zeta, \tau)$ and $\bar{\theta}_{\text{TDGL}}(\zeta, \tau)$, respectively, for the subcritical case ($\nu_0 = 0.26$), where we have used the same dimensionless time and the same scaling factors τ^* , a_ν^* , a_u^* , a_w^* , a_θ^* , $\zeta_u^*(\tau)$, $\zeta_w^*(\tau)$ and $\zeta_\theta^*(\tau)$ in Fig. 3.

- [2] T. Pöschel and S. Luding, eds., *Granular Gases* (Springer-Verlag, Berlin, 2001).
- [3] N. V. Brilliantov and T. Pöschel, *Kinetic Theory of Granular Gases* (Oxford University Press, Oxford, 2004).
- [4] I. Goldhirsch, *Annu. Rev. Fluid Mech.* **35**, 267 (2003).
- [5] H. Jeager, S. Nagel, and R. Behringer, *Rev. Mod. Phys.* **68**, 1259 (1996).
- [6] N. Sela, I. Goldhirsch, and S. H. Noskowitz, *Phys. Fluids* **8**, 2337 (1996).
- [7] A. Santos, V. Garzó, and J. W. Dufty, *Phys. Rev. E* **69**, 061303 (2004).
- [8] C. K. K. Lun, *J. Fluid Mech.* **233**, 539 (1991).
- [9] J. J. Brey, J. W. Dufty, C. S. Kim, and A. Santos, *Phys. Rev. E* **58**, 4638 (1998).
- [10] V. Garzó and J. W. Dufty, *Phys. Rev. E* **59**, 5895 (1998).
- [11] J. F. Lutsko, *Phys. Rev. E* **70**, 061101 (2004).
- [12] J. F. Lutsko, *Phys. Rev. E* **72**, 021306 (2005).
- [13] J. F. Lutsko, *Phys. Rev. E* **73**, 021302 (2006).
- [14] J. T. Jenkins and M. W. Richman, *Phys. Fluids* **28**, 3485 (1985).
- [15] J. T. Jenkins and M. W. Richman, *Arch. Ration. Mech. Anal.* **87**, 355 (1985).
- [16] M. L. Tan and I. Goldhirsch, *Phys. Fluids* **9**, 856 (1997).
- [17] K. Saitoh and H. Hayakawa, *Phys. Rev. E* **75**, 021302 (2007).
- [18] V. Kumaran, *Phys. Rev. Lett.* **96**, 258002 (2006).
- [19] V. Kumaran, *Phys. Rev. E* **79**, 011301 (2009).
- [20] V. Kumaran, *Phys. Rev. E* **79**, 011302 (2009).
- [21] A. Orpe and A. Kudrolli, *Phys. Rev. Lett.* **98**, 238001 (2007).
- [22] A. Orpe, V. Kumaran, K. Reddy, and A. Kudrolli, *Europhys. Lett.* **84**, 64003 (2008).
- [23] C. Rycroft, A. Orpe, and A. Kudrolli, *Phys. Rev. E* **80**, 031305 (2009).
- [24] J. F. Lutsko and J. W. Dufty, *Phys. Rev. A* **32**, 3040 (1985).
- [25] M. Otsuki and H. Hayakawa, *Eur. Phys. J. Special Topics* **179**, 179 (2009).
- [26] M. Otsuki and H. Hayakawa, *Phys. Rev. E* **79**, 021502 (2009).
- [27] M. Otsuki and H. Hayakawa, *J. Stat. Mech: Theor. Exp.* p. L08003 (2009).

- [28] M. Y. Louge, Phys. Fluids **6**, 2253 (1994).
- [29] M. Y. Louge, Phys. Rev. E **67**, 061303 (2003).
- [30] H. Xu, A. P. Reeves, and M. Y. Louge, Rev. Sci. Instrum. **75**, 811 (2004).
- [31] H. Xu, M. Y. Louge, and A. P. Reeves, Continuum Mech. Thermodyn. **15**, 321 (2003).
- [32] E. Khain, Phys. Rev. E **75**, 051310 (2007).
- [33] E. Khain, Eur. Phys. Lett. **87**, 14001 (2009).
- [34] G. D. R. Midi, Eur. Phys. J. E **14**, 341 (2004).
- [35] F. da Cruz, S. Eman, M. Prochnow, J. Roux, and F. Chevoir, Phys. Rev. E **72**, 021309 (2005).
- [36] T. Hatano, Phys. Rev. E **75**, 060301(R) (2007).
- [37] M. van Hecke, J. Phys. Condens. Matter **22**, 033101 (2010).
- [38] T. Hatano, M. Otsuki, and S. Sasa, J. Phys. Soc. Jpn. **76**, 023001 (2007).
- [39] T. Hatano, J. Phys. Soc. Jpn. **77**, 123002 (2008).
- [40] M. Otsuki and H. Hayakawa, Prog. Theor. Phys. **121**, 647 (2009).
- [41] M. Otsuki and H. Hayakawa, Phys. Rev. E **80**, 011308 (2009).
- [42] M. Otsuki, H. Hayakawa, and S. Luding, Prog. Theor. Phys. Suppl. **184**, 110 (2010).
- [43] M. Otsuki and H. Hayakawa, Phys. Rev. E **83**, 051301 (2011).
- [44] S. B. Savage, J. Fluid Mech. **241**, 109 (1992).
- [45] V. Garzó, Phys. Rev. E **73**, 021304 (2006).
- [46] P. J. Schmid and H. K. Kytömaa, J. Fluid Mech. **264**, 255 (1994).
- [47] C.-H. Wang, R. Jackson, and S. Sundaresan, J. Fluid Mech. **308**, 31 (1996).
- [48] M. Alam and P. R. Nott, J. Fluid Mech. **343**, 267 (1997).
- [49] M. Alam and P. R. Nott, J. Fluid Mech. **377**, 99 (1998).
- [50] B. Gayen and M. Alam, J. Fluid Mech. **567**, 195 (2006).
- [51] P. Shukla and M. Alam, Phys. Rev. Lett. **103**, 068001 (2009).
- [52] P. Shukla and M. Alam, J. Fluid Mech. **666**, 204 (2011).
- [53] P. Shukla and M. Alam, J. Fluid Mech. **672**, 147 (2011).
- [54] K. Saitoh and H. Hayakawa, Granular Matter **13**, 697 (2007).
- [55] A. W. Lees and S. F. Edwards, J. Phys. C **5**, 1921 (1972).
- [56] N. Mitarai, H. Hayakawa, and H. Nakanishi, Phys. Rev. Lett. **88**, 174301 (2002).
- [57] J. Jenkins and C. Zhang, Phys. Fluids **14**, 1228 (2002).
- [58] D. Yoon and J. Jenkins, Phys. Fluids **17**, 083301 (2005).
- [59] L. Verlet and D. Levesque, Mol. Phys. **46**, 969 (1982).
- [60] D. Henderson, Mol. Phys. **34**, 301 (1977).
- [61] D. Henderson, Mol. Phys. **30**, 971 (1975).
- [62] N. Carnahan and K. Starling, J. Chem. Phys. **51**, 635 (1969).
- [63] B. J. Glasser and I. Goldhirsch, Phys. Fluids **13**, 407 (2001).
- [64] C. Goldenberg and I. Goldhirsch, Phys. Rev. Lett. **89**, 084302 (2002).
- [65] I. Goldhirsch and C. Goldenberg, Eur. Phys. J. E **9**, 245 (2002).
- [66] C. Goldenberg and I. Goldhirsch, Granular Matter **6**, 87 (2004).
- [67] C. Goldenberg and I. Goldhirsch, Nature (London) **435**, 188 (2005).
- [68] C. Goldenberg, A. P. F. Atman, P. Claudin, G. Combe, and I. Goldhirsch, Phys. Rev. Lett. **96**, 168001 (2006).
- [69] I. Goldhirsch, Granular Matter **12**, 239 (2010).
- [70] J. Zhang, R. P. Behringer, and I. Goldhirsch, Prog. Theor. Phys. Suppl. **184**, 16 (2010).
- [71] A. H. Clark, P. Mort, and R. P. Behringer, Granular Matter **14**, 283 (2012).
- [72] T. Weinhart, A. R. Thornton, S. Luding, and O. Bokhove, Granular Matter **14**, 289 (2012).
- [73] Here, $\mathbf{q}(\tau) = \mathbf{q}_c + \delta\mathbf{q}(\tau) \equiv (\delta q, q_c - \epsilon t \delta q)$ and we use $\delta q \sim \epsilon$, thus the ζ component of $\mathbf{q}(\tau)$ is given by $q_\zeta(\tau) = q_c - \tau$.